Journal of Catalysis **206,** 295–304 (2002)
doi:10.1006/jcat.2001.3479, available online at http://www.idealibrary.com on IDEAL®

The Intrinsic Kinetics of *n*-Hexane Hydroisomerization Catalyzed by Platinum-Loaded Solid-Acid Catalysts

F. J. M. M. de Gauw,[1] J. van Grondelle, and R. A. van Santen

Schuit Institute of Catalysis, Eindhoven University of Technology, P.O. Box 513, 5600 MB Eindhoven, The Netherlands

Received August 23, 2001; revised November 14, 2001; accepted November 14, 2001

The hydroisomerization of *n*-hexane on a number of platinum-loaded acidic zeolites and Mg saponite was studied at atmospheric pressure, hydrogen to *n*-hexane molar ratios of 14–56, and temperatures of respectively 513–543 K (zeolites) and 583–613 K (saponite). Care has been taken to obtain initial data of fresh catalysts so that in comparisons between zeolites differences in deactivation rate can be excluded. By fitting the measured kinetic data to an equation based on the bifunctional mechanism and using independently obtained dehydrogenation and adsorption data it was possible to simultaneously determine the energy of protonation of hexene (ΔH_{prot}) and the activation energy of the elementary isomerization step ($E_{act,isom}$) as well as the corresponding preexponential factors. The range of observed values of both ΔH_{prot} and $E_{act,isom}$ are in agreement with results of quantum-chemical calculations. Even so, the variation in the $E_{act,isom}$ values was quite large (96–182 kJ/mol) in spite of the apparent uniformity in acid strength of the catalysts. This implies that lattice distortions required to accommodate the transition state depend sensitively on the structural and electronic environment of the acid site, which is different for each type of zeolite. A compensation effect was observed between the preexponential factor ν_{isom} of the isomerization rate constant and $E_{act,isom}$, as was shown by the fact that a plot of $\ln(\nu_{isom})$ versus $E_{act,isom}$ was linear. Therefore differences in overall kinetics between different zeolites are determined mainly by differences of adsorption constants of the reacting molecules.

Key Words: **hydroisomerization; intrinsic kinetics; bifunctional mechanism; zeolites; saponite; compensation effect.**

INTRODUCTION

Acid-catalyzed reactions of hydrocarbons are abundant in oil refining processes such as catalytic reforming and hydrocracking. The catalysts used for these processes are usually based on acidic zeolites. Knowledge of the mechanism and kinetics of these reactions is interesting from both a practical and a fundamentally scientific point of view. From a practical point of view, values of kinetic parameters are required for kinetic modeling, which is necessary for designing and optimizing commercial plants. From a fundamentally scientific point of view, kinetic measurements can be helpful in obtaining insight into the nature of the interaction between hydrocarbons and solid-acid sites and the relation between the pore structure of zeolites and the catalytic activity, in terms of both its effect on the adsorption properties of hydrocarbons and its effect on the structural and electronic properties of the acid sites. Here we present kinetic data of the hydroisomerization of *n*-hexane to iso-hexane catalyzed by different zeolites as well as by a nonporous synthetic clay. This reaction, which is one of the key reactions in oil reforming and is applied to increase the octane number of gasoline (branched alkanes have higher octane numbers than linear alkanes), has been chosen as a model acid-catalyzed reaction because of the relatively low rate of catalyst deactivation. This is due not only to the presence of excess hydrogen but also to the small amounts of platinum on the zeolite surface, which catalyzes the hydrogenation of coke precursors. The hydroisomerization reaction is generally accepted to take place according to the bifunctional mechanism proposed by Weisz (1), which is depicted in the following (for *n*-hexane as reacting molecule). As can be seen, the platinum function not only serves to suppress coke formation but also is actively involved in the mechanism as a (de)hydrogenation catalyst. This provides an alternative reaction path for alkane isomerization, which would otherwise involve the energetically much more unfavorable protonation of an alkane (2). The bifunctional scheme as depicted in Fig. 1 is somewhat misleading since it suggests that protonation of the alkene generates carbenium ions in the same way as occurs in liquid-phase superacids (3). However, quantum-chemical calculations have shown that protonation of alkenes on solid-acid sites renders so-called alkoxy species as stable reaction intermediates, which are bonded to the lattice by strong covalent C–O bonds (4–6). These calculations suggest that carbenium ion-like species only exist as a transition state of the (de)protonation reaction. Due to the formation of strong covalent bonds, the enthalpy of protonation (ΔH_{prot}) is expected to be accordingly high; the same holds for the activation energy of the isomerization step ($E_{act,isom}$) (step 4 in the bifunctional scheme)

[1] To whom correspondence should be addressed. Fax: (31) 40 245 5054. E-mail: F.J.M.M.de.Gauw@tue.nl.

0021-9517/02 $35.00

since this involves lengthening of the C–O bond. This is confirmed by results of quantum chemical (7–12) and kinetic model studies (13–15); values for ΔH_{prot} ranging from −46 kJ/mol (8) to −154 kJ/mol (15) and those for $E_{act,isom}$ ranging from 125 kJ/mol (14) to 190 kJ/mol (10) are reported. The values for $E_{act,isom}$ are indeed much higher than the corresponding values of 65–75 kJ/mol observed in liquid superacid solutions (16).

An intriguing issue that has thus far hardly been explored is what the effect of the environment of the acid site (for instance, the pore geometry) is on the kinetics. Most quantum-chemical calculations have been performed within the framework of a cluster approximation in which the zeolite is represented by a small fragment containing the acid site. In this cluster approach hydrogen atoms are used to compensate for the positive charge generated by cutting the tetrahedrally coordinated silicon atoms from the parent structure, and the geometries of the clusters are usually optimized as part of the calculation. As a result, the structural and electronic environments of the catalytic site are largely ignored, as pointed out by Sinclair *et al.* (11). As an alternative, these authors used a so-called embedded cluster model (17–19) to study alkene chemisorption on the acid sites of zeolite chabazite. In this model a quantum-chemical method is applied for the active-site region, and a classical method, which is computationally less demanding, is applied for the remainder of the system. The results showed that the stability of alkoxides is very sensitive to steric interactions with the local atoms of the acid site; that is, ΔH_{prot} is a function of the catalyst. So far this or other more sophisticated methods have not been used to calculate ΔH_{prot} for most zeolite structures, and the only experimentally determined value for ΔH_{prot} found in the literature was for isobutene protonation on zeolite Y (15). This uncertainty with regard to ΔH_{prot} values as determined by cluster model calculations also has implications for the reliability of experimentally determined values of $E_{act,isom}$. To calculate $E_{act,isom}$ from kinetic measurements, $E_{act,isom}$ is expressed as a function of a number of parameters (13, 14) including the apparent activation energy, which is the actually measured quantity, and ΔH_{prot}, for which nearly only quantum-chemical calculations are available. Therefore values for $E_{act,isom}$ determined in this way may also be unreliable. In conclusion, a meaningful kinetic analysis should involve an experimental determination of ΔH_{prot}. In the present study, the kinetic data are analyzed using a rate equation based on the bifunctional sheme in Fig. 1, which allows for the simultaneous determination of $E_{act,isom}$ and ΔH_{prot}. To distinguish between the effects of adsorption and the intrinsic kinetics on the reaction rate, independent adsorption data are used. The results obtained on the different zeolites are compared to each other and to the results of quantum-chemical calculations.

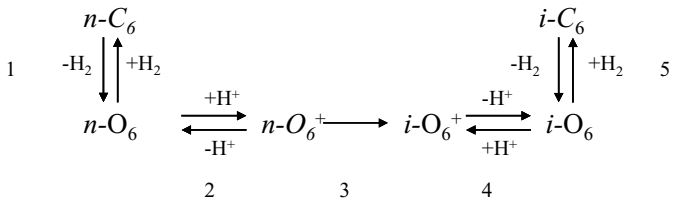

FIG. 1. Bifunctional scheme for hydroisomerization of *n*-hexane. C_6 = hexane, O_6 = hexene, O_6^+ = protonated hexene. The numbers refer to the elementary steps: 1, dehydrogenation/hydrogenation; 2, protonation/deprotonation; 3, isomerization; 4, deprotonation/protonation; 5, hydrogenation/dehydrogenation.

MEASUREMENT OF KINETIC DATA

Data Analysis

If it is assumed that the isomerization step is rate determining and the conversion is so low that the reverse reaction can be neglected,

$$\mathrm{TOF} = \frac{k_{isom}K_{ads}K_{dehydr}K_{prot}\frac{p_{n\mathrm{C}_6}}{p_{\mathrm{H}_2}}}{1 + K_{ads}p_{n\mathrm{C}_6} + K_{ads}K_{dehydr}\frac{p_{n\mathrm{C}_6}}{p_{\mathrm{H}_2}} + K_{ads}K_{dehydr}K_{prot}\frac{p_{n\mathrm{C}_6}}{p_{\mathrm{H}_2}}} \quad [1]$$

is obtained (20), where K_{ads}, K_{dehydr}, and K_{prot} are the equilibrium constants of, respectively, adsorption, dehydrogenation, and protonation of *n*-hexane; k_{isom} is the rate constant of conversion of the intermediate *n*-hexyl alkoxide into iso-hexyl alkoxide (no distinction is made between the various isomers); p_{H_2} is the hydrogen pressure; and $p_{n\mathrm{C}_6}$ is the *n*-hexane pressure. This equation can be made linear by taking the reciprocal

$$\frac{1}{\mathrm{TOF}} = \frac{1}{k_{isom}} + \frac{1}{k_{isom}K_{prot}} + \frac{p_{\mathrm{H}_2}}{k_{isom}K_{dehydr}K_{prot}} + \frac{p_{\mathrm{H}_2}}{k_{isom}K_{ads}K_{dehydr}K_{prot}}\frac{1}{p_{n\mathrm{C}_6}}. \quad [2]$$

Plots of 1/TOF versus $1/p_{n\mathrm{C}_6}$ should be linear, and since K_{ads} and K_{dehydr} are known or can be determined from independent experiments, k_{isom} and K_{prot} can be calculated from the slope (s) and intercept (i):

$$k_{isom} = \frac{p_{\mathrm{H}_2}}{ip_{\mathrm{H}_2} - sK_{ads}p_{\mathrm{H}_2} - sK_{ads}K_{dehydr}} \quad [3]$$

$$K_{prot} = \frac{ip_{\mathrm{H}_2}}{sK_{ads}K_{dehydr}} - \frac{p_{\mathrm{H}_2}}{K_{dehydr}} - 1. \quad [4]$$

By determining k_{isom} and K_{prot} in the previously described manner as a function of temperature and plotting $\ln(k_{isom})$ and $\ln(K_{prot})$ versus the reciprocal temperature, respectively, $E_{act,isom}$ and ΔH_{prot} can be obtained.

Measurement of Intrinsic Kinetics

To ascertain that Eq. [1] adequately describes the experimental results, it should be determined whether the conditions are fulfilled under which Eq. [1] is valid. The condition that the isomerization step is rate limiting implies in the first place that the dehydrogenation/hydrogenation equilibrium is established, which means that the concentration of platinum relative to the concentration of acid sites is so high, that in the per unit of catalyst mass, the rate of (de)hydrogenation is much higher than the rate of *n*-alkoxide conversion. The common way to verify this is by preparing catalysts with varying platinum loading and comparing the reaction rates; if the activity does not increase with metal loading, it can be assumed that the dehydrogenation/hydrogenation steps are equilibrated. In the second place, it should be verified that mass transfer is not rate limiting. For the biporous catalyst used in this study, mass transfer can be subdivided into three types, namely, transport through the film surrounding the catalyst pellets, macropore diffusion, and micropore diffusion. A common test for film mass transfer limitation is to vary the flow rate at constant space–time (21); if the conversion does not change it can be assumed that film mass transfer is not rate limiting. This test is based on the fact that the rate of mass transfer is a function of the thickness of the film, which in turn is a function of the flow rate. If film mass transfer limitation is absent, the conversion X measured under differential conditions is inversely proportional to the flow rate F. Therefore, as an alternative test, XF is measured as a function of F, and the critical flow rate F_c is determined at which XF becomes constant. It can be assumed that for flow rates higher than F_c film mass transfer is not rate limiting.

Since the mean residence time of molecules within a catalyst particle is proportional to the square of the particle diameter (22), macropore diffusion limitation leads to a decrease in activity with an increase in pellet diameter. Therefore, if the activity of two catalysts with a different pellet diameter is equal, macropore diffusion limitation can be excluded. By analogy, micropore diffusion limitation will lead to a dependence of the activity on the diameter of the crystals, so the corresponding test would be to compare the activities on samples with different crystal sizes.

A final possible source of deviation from the intrinsic kinetics is deactivation. Deactivation is mainly caused by coke formation, which results from oligomerization of intermediate alkenes. Therefore, the alkene concentration should be kept low to suppress deactivation, which is done in industrial reforming by applying high hydrogen pressure (~10–30 bar). In this study, however, the experiments were performed at atmospheric pressure, so deactivation may have a significant effect. The effect of deactivation on the catalytic activity is very difficult to assess, because

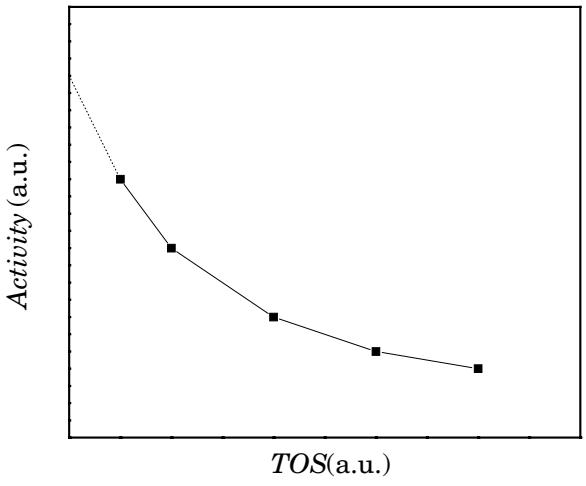

FIG. 2. Estimation of the catalytic activity in case of absence of deactivation by extrapolation to zero time on stream.

the level of deactivation is at least a function of time, temperature, and hexane concentration. Also it is known that there is no unambiguous relation between the level of coking, which can be measured, and the catalytic activity (23), making later corrections based on this method unreliable. A relatively easy way to solve this problem is by estimating the activity of the catalyst if *it were not deactivated* by extrapolation of plots of conversion versus time on stream (TOS) to TOS = 0. This is illustrated in Fig. 2. The catalyst is regenerated before measuring at new values of the temperature or *n*-hexane pressure. It is important to emphasize that the meaning of the value thus obtained is the steady-state activity of the catalyst *if deactivation were absent*. This is not the same as an activity that would actually be measured at TOS = 0, because this value would include other run-in effects such as an incomplete establishment of the equilibrium between the gas phase and the adsorbed molecules.

For each temperature and *n*-hexane pressure only one measurement was performed at TOS = 5 min to limit the number of measurements, and the measured activity was representative of the activity at TOS = 0. The error caused by this approximation was relatively small, as was demonstrated by the fact that activities determined by extrapolation of activity versus TOS plots were less than 5% higher than those measured at TOS = 5 min.

Determination of Dehydrogenation and Adsorption Parameters

The dehydrogenation parameters, the dehydrogenation enthalpy (ΔH_{dehydr}) and the preexponential factor of K_{dehydr} ($K_{dehydr}{}^0$), were calculated from the standard enthalpy and entropy of formation of *n*-hexane and the

average standard enthalpy and entropy of formation of all unbranched hexene isomers;

$$\Delta H_{dehydr} \approx \Delta H_{f,hexene}{}^{\theta} - \Delta H_{f,n-hexane}{}^{\theta} \quad [5]$$

$$K_{dehydr}{}^{0} \approx p^{\theta} \exp\left(\frac{\Delta S_{f,hexene}{}^{\theta} - \Delta S_{f,n-hexane}{}^{\theta}}{R}\right), \quad [6]$$

where $\Delta H_{f,i}{}^{\theta}$ and $\Delta S_{f,i}{}^{\theta}$ are, respectively, the standard enthalpy and entropy of formation of compound i in the gas phase (the temperature dependence of $\Delta H_{f,i}{}^{\theta}$ and $\Delta S_{f,i}{}^{\theta}$ was neglected), and p^{θ} is the standard pressure ($p^{\theta} = 101{,}325$ Pa). The values of $\Delta S_f{}^{\theta}$ and $\Delta H_f{}^{\theta}$ of *n*-hexane and "hexene" were extracted from Ref. (24). Although K_{dehydr} refers to the adsorbed phase and $\Delta H_{f,i}{}^{\theta}$ and $\Delta S_{f,i}{}^{\theta}$ refer to the gas phase, it is assumed that the difference between the formation enthalpy/entropy in the gas phase and in the adsorbed phase is equal for *n*-hexane and "hexene," so that the enthalpy/entropy of dehydrogenation is equal in both phases. (The calculations in Eqs. [5] and [6] can be safely made, since the values for the individual isomers vary by less than 10%.)

The adsorption parameters for all materials except H-beta and Mg-saponite were taken from studies published by Eder and Lercher (25, 26). The preexponential factors (in units Pa^{-1}) were calculated from the Henry constants K_H (in units mmol/g · atm) measured at temperature T_m using

$$K_{ads}{}^{0} = \frac{K_H(T_m)}{p^{\theta} Q_{max} \exp\left(-\frac{\Delta H_{ads}}{RT_m}\right)}, \quad [7]$$

where Q_{max} denotes the maximum concentration of *n*-hexane in the porous crystals (in units mol/kg). The values of Q_{max} for H-mordenite, H-ZSM-5, and H-ZSM-22 were extracted from the literature (25, 26). As no literature values were found with regard to saponite and H-beta, the adsorption parameters of these materials were determined by means of pulse chromatography. From the concentration distribution measured at the outlet of the reactor a dimensionless adsorption constant $K_{ads}{}^{*}$ can be calculated (for bidisperse solids) using

$$\mu = \frac{\tau}{2} + \frac{L}{v}[\varepsilon_z + (1-\varepsilon_z)\varepsilon_y + (1-\varepsilon_z)(1-\varepsilon_y)\varepsilon_x(1+K_{ads}{}^{*})], \quad [8]$$

which is valid for linear adsorption isotherms (27), where μ = first moment of the concentration distribution function measured at the column outlet, τ = width of the input pulse, L = column length, v = velocity of the carrier gas, ε_x = porosity (fraction consisting of void space) of the crystals, ε_y = porosity of the pellets, and ε_z = porosity of the column. K_{ads} can be calculated from $K_{ads}{}^{*}$,

$$K_{ads} = \frac{\varepsilon_x K_{ads}{}^{*}}{Q_{max}\rho RT}, \quad [9]$$

where ρ = density of the crystals including the micropores. The values of Q_{max} for H-beta and Mg-saponite were determined by measuring the adsorption isotherm at a suitable temperature and extrapolating the linear part to $p = 0$.

METHODS AND MATERIALS

Catalyst Preparation

A sample of the synthetic clay Mg-saponite (loaded with 2 wt% of platinum) and samples of the zeolites NH_4-Beta, Na-Beta, Na-ZSM-5, Na-ZSM-22, and Na-mordenite were kindly donated by Exxon Chemicals in Machelen, Belgium; Shell Research and Technology Centre in Amsterdam, The Netherlands; and Akzo-Nobel, The Netherlands. The sodium zeolites were converted into the ammonium form by repeated (three times) ion exchange at room temperature for 16 h in a 1 M solution of ammonium nitrate in water. The proton form was prepared by calcination of the ammonium zeolites in flowing air at 773 K. Subsequently a part of the protons was exchanged for Pt^{2+} ions in a watery solution of platinum(II)tetra-ammonium hydroxide for 16 h at room temperature. The solution contained exactly the amount of platinum corresponding to the desired loading upon complete exchange. The filtrate was checked for platinum by UV–vis (28); platinum was not detected in any of the filtrates, indicating that in all cases exchange was complete. After drying at 60°C the samples were carefully calcined by heating at a rate of 0.5 K/min to 450°C in flowing air and maintaining this temperature for 2 h. Finally the samples were reduced in flowing hydrogen for 2 h at 400°C.

As mentioned in the Introduction, a straightforward method of gauging whether the hydrogenation/dehydrogenation reactions are equilibrated is to compare the reaction rates for catalysts with different platinum loading. To decide whether micropore diffusion limitation occurs, the activities of catalysts with different crystal sizes should also be compared. This would require the preparation of four catalysts for each zeolite type that is studied. To limit the amount of catalysts to be prepared, for each type of zeolite two catalysts with different platinum loadings (catalysts 1 and 2) were prepared from one starting material, whereas only one catalyst (catalyst 3) was prepared from the other material. Catalyst 3 was loaded with such an amount of platinum that it had a higher platinum-to-acid site ratio than at least one of the other two catalysts. Therefore, if the activities of catalysts 1 and 2 do not differ significantly, it can be assumed for all three catalysts that the hydrogenation/dehydrogenation reactions are equilibrated.

Catalyst Characterization

The crystal size of the samples was determined by scanning electron microscopy. The strength of the acid sites of the samples was determined by infrared spectroscopy using

a Nicolet Protégé 460 FT–IR spectrometer equipped with a diffuse reflectance accessory. As pointed out by Kazansky (29), the only proper way to determine the acid strength of surface OH groups with IR is by studying their interaction with adsorbed bases. To probe the interaction between acid sites and a reactant realistically, it is necessary to use a base that has a hardness similar to that of the reactant (30). In this study 1-butene was chosen as a probe molecule. As a measure of acid strength the shift of the maximum of the peak corresponding to the OH stretch vibration of the Brønsted acid site upon 1-butene adsorption was taken. The void OH vibration band is positioned at about 3610 cm^{-1}, whereas the perturbed OH vibration band is centered at around 3100 cm^{-1} (31). The catalysts were activated by heating to 450°C in flowing hydrogen and maintaining this temperature for 1 h. Subsequently the temperature was lowered to room temperature and a spectrum was recorded. Then a flow of 1-butene was added to the hydrogen flow and a second spectrum was recorded, also at room temperature.

The concentration of Brønsted acid sites of the materials (with exception of Pt/Mg-saponite) was determined by temperature-programmed decomposition of isopropylamine (TPDI). In contrast to temperature-programmed desorption of ammonia, this method allows for the selective determination of the concentration of sites which are active in hydrocarbon conversion. With increasing temperature isopropylamine molecules adsorbed on these sites will crack to form propene and ammonia, whereas molecules adsorbed on other acid sites will desorb without decomposing (32). A tube reactor loaded with about 100 mg of the sample (sieve fraction 125–500 μm) was dried for 2 h in helium at 450°C, and after cooling to 100°C *it was* exposed to a flow of helium saturated at 0°C with isopropylamine. Then excess physisorbed isopropylamine was removed at 100°C in flowing helium (200 Nml/min) for 16 h, and subsequently the temperature was increased to 500°C. The concentrations of the released products were monitored with mass spectrometry ($m/e = 44$ for isopropylamine and $m/e = 41$ for propene). Since every Brønsted acid site can adsorb one isopropylamine molecule, the amount of propene released equals the amount of Brønsted acid sites.

As the (de)hydrogenation activity is determined by the concentration of surface platinum, it is essential to verify that this concentration is indeed varied with changing bulk concentration to be able to judge whether the hydrogenation/dehydrogenation steps are equilibrated. The conventional method to determine the concentration of surface metal is chemisorption of hydrogen, oxygen, or carbon monoxide. However, it was found that the catalysts did not adsorb significant amounts of any of these probes at room temperature, although they were catalytically active. This is in accordance with the results of chemisorption measurements obtained for other metal-loaded zeolites (33–35), which demonstrated that the amount of adsorbed hydrogen decreases with increasing acidity of the supporting zeolite. Moreover, results of IR measurements showed that the frequency of adsorbed CO molecules on ruthenium-loaded zeolites tends to increase with increasing acidity (36), indicating a weakening of the metal–CO bond. These observations were connected to the formation of bonds between metal particles and protons (37, 38). According to this model protons and probe molecules compete for the same ligand positions of the particles, so that with increasing proton concentration and strength the fraction of ligand positions occupied by probe molecules decreases.

As an alternative to chemisorption, the gas-phase 1-hexene hydrogenation activity of all catalysts was determined and divided by the concentration of acid sites. This quantity was taken as a measure of the concentration of catalytically active platinum sites relative to the concentration of acid sites. As in the hydroisomerization experiments, the measurements were carried out after TOS = 5 min to limit the effect of deactivation on the measured activities.

The results of the catalyst characterization are given in Table 1. The shifts of the OH stretch vibration frequencies upon 1-butene adsorption varied between 501 and 517 cm^{-1}, indicating that the strength of the acid sites was similar for all samples. For all types of zeolites the hydrogenation activity of catalyst 3 was higher than that of at least one of the catalysts 1 and 2, as intended (see *Catalyst Preparation*).

Equipment

The measurements were carried out using a continuous flow reactor, consisting of a 4-mm-i.d. quartz tube reactor that was filled with zeolite pellets and placed inside an oven. Gas-phase mixtures of *n*-hexane (Merck, >99%) and hydrogen were obtained using a Bronckhorst CEM (Controller/Evaporator/Mixer) unit, consisting of a liquid mass flow controller for *n*-hexane, a mass flow controller for hydrogen, and a heated mixing chamber. An additional mass flow controller was used for adding controlled amounts of nitrogen to be able to vary alkane concentrations at constant hydrogen pressure and space velocity. The gas mixtures were passed through the catalyst bed, and the reaction products were analyzed online with a HP5890 Series II gas chromatograph containing a Chrompack fused silica column with Al_2O_3/KCl coating and a flame ionization detector.

Conditions

The measurements were carried out at atmospheric pressure and at temperatures between 513 and 543 K; measurements on Mg-saponite were carried out at temperatures between 583 and 613 K because of the much lower catalytic activity. A total flow of 150 Nml/min was used, consisting of 140 Nml/min hydrogen, 2.5–10 Nml/min *n*-hexane, and

TABLE 1

Results of Catalyst Characterization[a]

Catalyst	Si/Al ratio	L (μm)	$\Delta\nu_{OH}$ (cm^{-1})	C_H^+ (mol/g)	Pt loading (wt%)	A_{hydr}/C_H^+ (mol 1-hexene/s/mol H$^+$)
Beta 1	14	0.1–0.5	n.d.[b]	7.2×10^{-4}	1.6	4.0×10^{-3}
Beta 2	14	0.1–0.5	n.d.	7.2×10^{-4}	2.2	1.6×10^{-2}
Beta 3	12.5	1	513	9.7×10^{-4}	2	5.1×10^{-3}
Mordenite 1	35	0.01–0.1	n.d.	3.3×10^{-4}	2	2.0×10^{-2}
Mordenite 2	10	0.5–1	512	5.0×10^{-4}	2	1.2×10^{-2}
Mordenite 3	10	0.5–1	n.d.	5.0×10^{-4}	3	2.2×10^{-2}
ZSM-5 #1	28	0.6	517	5.5×10^{-4}	1	4.0×10^{-3}
ZSM-5 #2	28	3.5	n.d.	4.9×10^{-4}	0.5	3.9×10^{-3}
ZSM-5 #3	28	3.5	n.d.	4.9×10^{-4}	1	7.8×10^{-3}
ZSM-22 #1	39	1–2	n.d.	2.2×10^{-4}	0.5	2.5×10^{-2}
ZSM-22 #2	39	1–2	501	2.2×10^{-4}	0.7	8.0×10^{-2}
ZSM-22 #3	35	4	n.d.	1.1×10^{-4}	0.7	5.4×10^{-2}
Mg-saponite	5.5	—	—[c]	4.3×10^{-6}[d]	2	—

[a] C_H^+ = concentration of Brønsted acid sites, L = crystal size, $\Delta\nu_{OH}$ = shift of the Brønsted OH stretch vibration frequency, A_{hydr} = 1-hexene hydrogenation activity at $T = 50°C$, $p = 100$ kPa, and $p_{H_2}/p_{1\text{-}hexene} = 20$.

[b] Not determined.

[c] Adsorption was below detection limit.

[d] Determined from IR absorbance of OD bonds generated by selective deuteration of Brønsted acid sites using perdeuterobenzene (M. S. Rigutto *et al.*, in preparation).

0–7.5 Nml/min nitrogen. The reactor was filled with zeolite pellets, between 125 and 250 μm in diameter, which were obtained by compressing, crushing, and sieving. As the differential method of kinetic analysis was used, the amounts of catalyst were tuned to keep conversions below 10%.

As mentioned earlier, individual activity measurements were performed after a 5-min time on stream to minimize the influence of deactivation on the measured activity. After each activity measurement, the catalyst was regenerated at 450°C in flowing hydrogen for 2 h.

The TOF's that were used for data analysis were calculated from the total conversion toward all hexane isomers and propane, which is a secondary product since it is predominantly formed by cracking of branched isomers.

Measurements regarding the assessment of the effects of mass transfer and the relative (de)hydrogenation activity on the reaction rate were carried out at both the lower and the upper value of the range of temperatures used in the kinetic experiments. The effect of film mass transfer and macropore diffusion on the hydroisomerization activity was studied for the catalyst with the highest activity per unit of volume, Pt/H-beta, because if no mass transfer limitation was observed in this case, it could be safely assumed that the same would be true for the less active catalysts.

RESULTS AND DISCUSSION

Experiments Concerning the Influence of Mass Transfer and (De)hydrogenation Activity

The influence of film mass transfer was studied by measuring XF as a function of F for catalyst beta 2 at 270°C and $p_{H_2}/p_{nC_6} = 14$. Within the range of flows examined (50–150 Nml/min) no significant increase of activity was observed, so that film mass transfer limitation could be excluded at the flow rate that was applied during the kinetic measurements (150 Nml/min).

The effect of macropore diffusion on the hydroisomerization kinetics was investigated by comparing the activities of two samples of Beta 2, consisting of pellets with a diameter of, respectively, 125–250 and 250–500 μm, at the same temperature (270°C), flow rate (150 Nml/min), and p_{H_2}/p_{nC_6} (31). The measured activities differed by less than 10%, which is within the experimental margin of error. Therefore it was concluded that macropore diffusion was not rate limiting.

Table 2 represents the results of the measurements that were carried out to study the influence of micropore diffusion and the (de)hydrogenation activity on the hydroisomerization kinetics. For all zeolites the hydrogenation/dehydrogenation steps appeared to be equilibrated, as indicated by the fact that the activities of each of the two catalysts compared in these experiments were equal within about 10%. The results of the experiments regarding the influence of micropore diffusion displayed a small difference in the activities of the ZSM-5 and ZSM-22 catalysts (less than about 10%), but a large difference in the activities of beta and mordenite catalysts. However, for both zeolites the variation of the activity ratio with temperature was relatively small; i.e., the apparent activation energy did not seem to be a function of crystal size. This suggests that the activity differences did not result from diffusion limitation, since the apparent activation energy either decreases (20) or, as is possible in the case of *single-file* diffusion

TABLE 2

Results of Measurements Regarding Influence of Micropore Diffusion and (De)hydrogenation Activity on Hydroisomerization Kinetics

Type of influence studied	Catalysts involved	$\frac{\text{TOF catalyst 1}}{\text{TOF catalyst 2}}$ (240°C)	$\frac{\text{TOF catalyst 1}}{\text{TOF catalyst 2}}$ (270°C)
(De)hydrogenation activity	Beta 1 Beta 2	1.1	1.0
Micropore diffusion	Beta 1 Beta 3	2.0	1.6
(De)hydrogenation activity	Mordenite 2 Mordenite 3	0.89	0.93
Micropore diffusion	Mordenite 1 Mordenite 3	0.14	0.14
(De)hydrogenation activity	ZSM-5 #2 ZSM-5 #3	0.93	0.91
Micropore diffusion	ZSM-5 #1 ZSM-5 #3	1.1	1.1
(De)hydrogenation activity	ZSM-22 #1 ZSM-22 #2	1.1	1.0
Micropore diffusion	ZSM-22 #2 ZSM-22 #3	0.91	0.88

(diffusion in one-dimensional pores such as those of mordenite in which the adsorbed molecules cannot pass each other), increases when the degree of diffusion limitation increases (39). Of course diffusion limitation cannot explain the differences observed for mordenite, since the catalyst with the smaller crystal size was less active than the catalyst with the larger crystal size instead of the other way round. On the basis of these experiments one can only speculate about the reasons for the observed differences for beta and mordenite. Here we will confine ourselves to remarking that the apparent variation in the activity of different samples of the same zeolite adds to the error in the values of the preexponential factors of k_{isom} and K_{prot} as determined from kinetic measurements. However, the values of $E_{act,isom}$ and ΔH_{prot} were hardly affected, since the differences did not vary much with temperature.

Dehydrogenation and Adsorption Parameters

The dehydrogenation parameters were calculated using Eqs. [5] and [6] and thermodynamic data taken from Ref. (24); this resulted in $K_{dehydr}{}^0 = 4.17 \times 10^{11}$ Pa and $\Delta H_{dehydr} = 118$ kJ/mol. The adsorption parameters are given in Table 3. The adsorption enthalpy measured for H-beta was 8 kJ/mol higher than the value measured by Denayer *et al.* (40) for Na-beta, presumably as a result of the presence of acid sites, which are known to enhance the adsorption energy (41).

Kinetic Measurements

The catalysts that were used for kinetic measurements were beta 3, mordenite 3, ZSM-5 #1, ZSM-22 #2, and the platinum-loaded Mg-saponite. The results are shown in Fig. 3 and Table 4. ($K_{prot}{}^0$ and ν_{isom} are the preexponential factors of, respectively, K_{prot} and k_{isom}.) The measured protonation energies are all well within the range of quantum chemically calculated protonation energies (8–12, 42). Nevertheless the ΔH_{prot} values vary over about 20 kJ/mol,

TABLE 3

Adsorption Parameters

Material	$K_{ads}{}^0$ (Pa^{-1})	ΔH_{ads} (kJ/mol)
H-beta	1.5×10^{-12}	−71
H-mordenite	1.4×10^{-11}	−69
H-ZSM-5	6.2×10^{-14}	−82
H-ZSM-22	6.3×10^{-14}	−82
Mg-saponite	1.1×10^{-9}	−34

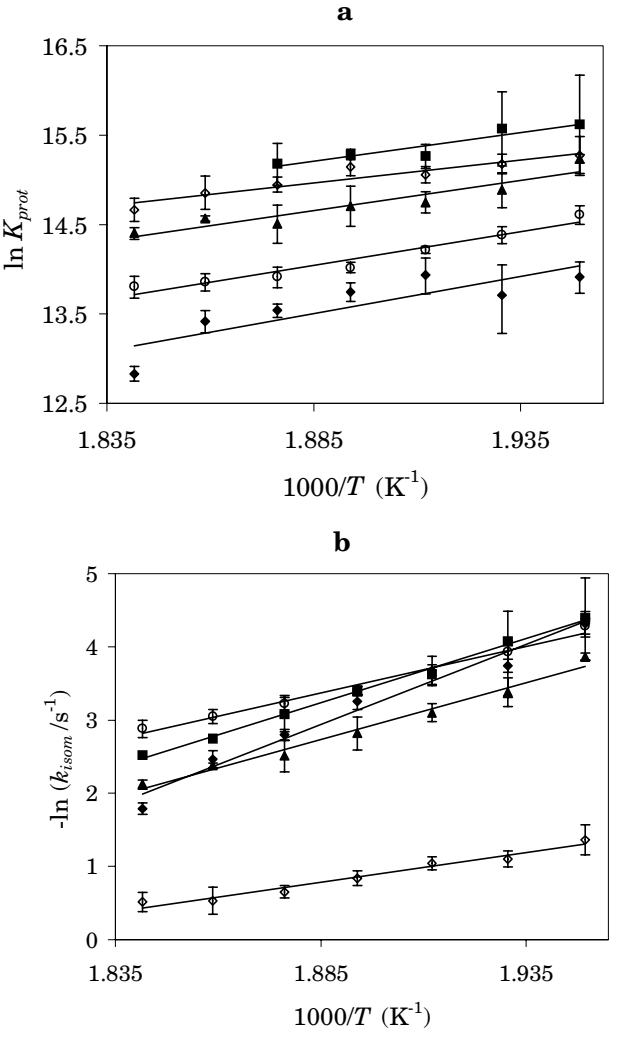

FIG. 3. Determination of kinetic parameters. (a) ln K_{prot} versus reciprocal temperature. (b) ln k_{isom} versus reciprocal temperature (◆, beta; ▲, mordenite, ■, ZSM-5; ○, ZSM-22; ◇, saponite).

TABLE 4

Results of Kinetic Measurements

Catalyst	ν_{isom} (s^{-1})	$E_{act,isom}$ (kJ/mol)	$K_{prot}{}^{0}$ (–)	ΔH_{prot} (kJ/mol)
Beta 3	$10^{16.6\pm1.4}$	182 ± 14	$10^{-1.0\pm1.9}$	-69 ± 19
Mordenite 3	$10^{11.6\pm0.8}$	129 ± 8	$10^{0.8\pm0.9}$	-56 ± 9
ZSM-5 #1	$10^{13.0\pm0.4}$	146 ± 4	$10^{1.3\pm1.2}$	-53 ± 12
ZSM-22 #2	$10^{8.9\pm0.6}$	106 ± 6	$10^{-0.1\pm0.7}$	-63 ± 7
Mg-saponite	$10^{8.0\pm0.5}$	96 ± 6	$10^{1.7\pm0.7}$	-55 ± 8

indicating some influence of the structural and electronic environment of the acid site. This variation is smaller than that found by Sinclair *et al.* for a series of alkoxides in the pores of chabazite (11). However, in the case of chabazite the influence of steric repulsions is probably much stronger due to the relatively small pore size (3.8 × 3.8 Å versus 4.4 × 5.5 Å for ZSM-22, which has the smallest pores of the four zeolites studied here). Compared with the variation in ΔH_{prot} values, the variation in $E_{act,isom}$ values is huge. Moreover, the values of ΔH_{prot} and $E_{act,isom}$ appear to be unrelated, whereas one would expect that $E_{act,isom}$ would increase with increasing $-\Delta H_{prot}$. (A higher value of $-\Delta H_{prot}$ implies that the alkoxy ground state is more stable.) Therefore it was concluded that the differences are connected to differences in the stability of the transition state. Since formation of the transition state in acid-catalyzed hydrocarbon reactions involves a partial transfer of the hydrogen atom of the acid site's OH group to the hydrocarbon fragment (4, 8), the activation energy decreases with increasing acidity (8, 10). Hence, an explanation for the large variation in $E_{act,isom}$ values could be that there is a dissimilarity in the strength of the acid sites of the various samples. As mentioned previously, the results of IR measurements showed that the acid strength of all samples was similar. However, upon closer consideration it can be questioned whether the relation between $\Delta\nu_{OH}$ and $E_{act,isom}$ is independent of zeolite structure. In essence $\Delta\nu_{OH}$ is a measure of the stability of the π-complex relative to the adsorbed alkene, whereas $E_{act,isom}$ can be considered as the difference in stability between the carbenium ion-like transition state and the starting alkoxide. Since the variation in protonation energies was found to be only about 20 kJ/mol, it can be concluded that the relative stabilities of the adsorbed alkene and the alkoxide are not strong functions of the catalyst. Therefore the variation in $E_{act,isom}$ values for the same (apparent) acidity is probably due to variations in the energy difference between the π-complex and the transition state of the isomerization step. This variation may be related to differences in the energy changes that are involved in the distortion of the catalytic site necessary to accommodate, respectively, the π-complex and the transition state of the isomerization step. According to quantum-mechanical cluster calculations the optimized geometry of the cluster in the π-complex differs considerably from that in the transition state (9). Of course the same holds true for real catalytic sites, and the changes in geometry and the accompanying changes in energy are functions of the spatial and electronic structures of the catalytic site. Since a zeolite usually contains several crystallographically different tetrahedral sites, there may even be differences within the same zeolite structure. As a result, an appropriate way to explain the observed differences in $E_{act,isom}$ is by performing quantum-chemical calculations using models that explicitly take into account the specific environment of the acid sites, such as the aforementioned embedded cluster models.

In view of the large variation in $E_{act,isom}$ values, the variation in the TOF's as measured on the various catalysts is surprisingly small: within the range of experimental conditions used in this study the lowest and highest TOFs at a given *n*-hexane pressure and temperature differed only by a factor of between 4 and 17. (Note: the range of temperatures referred to here is 240–270°C; the TOFs on Mg-saponite were measured at higher temperatures, so the TOFs in the range 240–270°C had to be calculated using the experimentally obtained kinetic parameters.) If the influence of differences in the adsorption parameters were taken into account; that is, if only the values of k_{isom} were considered, the variation would be even less: the highest k_{isom} value would exceed the lowest by a factor of between 2.0 and 2.5. This indicates that, under the experimental conditions used here, the observed differences in TOF values are primarily caused by differences in the adsorption constants and that there is a compensation effect between ν_{isom} and $E_{act,isom}$. Indeed, if $\ln(\nu_{isom})$ were plotted as a function of $E_{act,isom}$ a straight line would be obtained (see Fig. 4), although a single isokinetic temperature could not be defined. However,

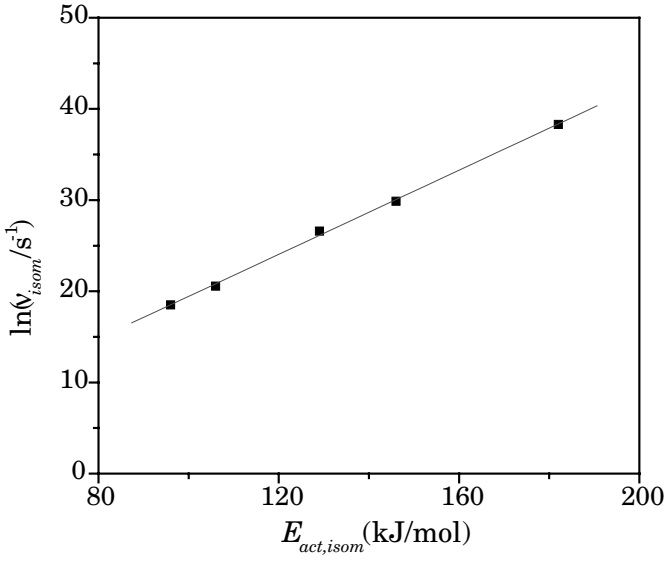

FIG. 4. $\ln(\nu_{isom})$ as a function of $E_{act,isom}$.

the small variation in k_{isom} values within the experimental temperature range suggests that the temperature at which the variation is minimal is within or just outside this range. Indeed, this temperature was found to be equal to 244°C. This means that at the temperature of industrial hydroisomerization [230–280°C (43)] the contribution of differences in k_{isom} to the differences in activity (in mol/g) between various catalysts is relatively small. Moreover, at the pressures that are used [14–41 bar total at a hydrogen-to-hydrocarbon ratio of 1–4 mol/mol (42)] the surface occupancy of alkoxides is close to 1 which means that adsorption effects can be neglected. This leads to the conclusion that under industrial conditions differences in catalytic activity between catalysts are predominantly determined by differences in the concentration of acid sites (at least for equal apparent strength of the acid sites). Of course, this statement is only valid if the influence of deactivation is not considered, since differences in deactivation behavior between catalysts may lead to quite different steady-state activities. The second restriction that must be made is that the compensation effect that was found does not necessarily apply to catalysts not studied here.

CONCLUSIONS

By measuring the rate of the *n*-hexane hydroisomerization reaction on various platinum-loaded acidic catalysts (the zeolites H-beta, H-mordenite, H-ZSM-5, H-ZSM-22, as well as the synthetic clay Mg-saponite) as a function of *n*-hexane pressure and fitting the results to a rate equation based on the bifuctional isomerization scheme of Weisz, it was possible to simultaneously determine the equilibrium constant of hexene protonation and the rate constant of isomerization of the resulting *n*-hexyl alkoxides. By repeating this procedure at different temperatures the protonation energy ΔH_{prot}, the activation energy of isomerization $E_{act,isom}$, and the corresponding preexponential factors could be determined. The measured values of ΔH_{prot} varied between −53 and −69 kJ/mol, whereas the values of $E_{act,isom}$ varied between 96 and 182 kJ/mol. The range of ΔH_{prot} and $E_{act,isom}$ values agrees well with the results of quantum-chemical calculations, although the variation in $E_{act,isom}$ values is striking. As the (apparent) strength of the acid sites of all catalysts was equal, this variation is probably related to the precise electronic and geometrical changes involved in the formation of the transition state, which are specific of the catalyst and even of the crystallographic position of the acid site. Quantum-chemical calculations that explicitly take the environment of the acid site into account (for instance, by using embedded cluster models) are required to explain these results. A compensation effect was found between $E_{act,isom}$ and the corresponding preexponential factor, although an isokinetic temperature could not be established. Even so, within the experimental range of temperatures (240–270°C) the variation in isomerization reaction rate constants (k_{isom}) was relatively small, leading to the conclusion that differences in turnover frequencies (TOF) observed for the various catalysts were predominantly caused by differences in the adsorption constants. Since the temperature range at which industrial hydroisomerization is operated is more or less the same as that used here and since it can be shown that at the pressures that are applied in the industrial process the surface occupancy of alkoxides is close to 1, it is concluded that differences in catalytic activity (in units mol/g) are mainly governed by the concentration of acid sites, provided that the strength of the acid sites is comparable and differences in deactivation behavior can be neglected.

REFERENCES

1. Weisz, P. B., *in* "Advances in Catalysis and Related Subjects" (D. D. Eley, P. W. Selwood, and P. B. Weisz, Eds.), Vol. 13, p. 137. Academic Press, New York, 1962.
2. Jacobs, P. A., and Martens, J. A., *Stud. Surf. Sci. Catal.* **58**, 445 (1991).
3. Brouwer, D. M., *in* "Chemistry and Chemical Engineering of Catalytic Processes" (R. Prins and G. C. A. Schuit, Eds.), pp. 137–160. Sijthoff & Noordhoff, Alphen aan de Rijn, The Netherlands, 1980.
4. Kazansky, V. B., and Senchenya, I. N., *J. Catal.* **119**, 108 (1989).
5. Senchenya, I. N., and Kazansky, V. B., *Catal. Lett.* **8**, 317 (1991).
6. Van Santen, R. A., and Kramer, G. J., *Chem. Rev.* **95**, 637 (1995).
7. Kazansky, V. B., Frash, M. V., and Van Santen, R. A., *Appl. Catal. A Gen.* **146**, 225 (1996).
8. Rigby, A. M., Kramer, G. J., and Van Santen, R. A., *J. Catal.* **170**, 1 (1997).
9. Boronat, M., Viruela, P., and Corma, A., *J. Phys. Chem. A* **102**, 982 (1998).
10. Natal-Santiago, M. A., Alcalá, R., and Dumesic, J. A., *J. Catal.* **181**, 124 (1999).
11. Sinclair, Ph. E., De Vries, A., Sherwood, P., Catlow, R. A., and Van Santen, R. A., *J. Chem. Soc., Faraday Trans.* **94**, 3401 (1998).
12. Viruela-Martín, P., Zicovich-Wilson, C. M., and Corma, A., *J. Phys. Chem.* **97**, 13713 (1993).
13. Martens, G. G., Marin, G. B., Martens, J. A., Jacobs, P. A., and Baron, G. V., *J. Catal.* **195**, 253 (2000).
14. Van de Runstraat, A., Kamp, J. A., Stobbelaar, P. J., Van Grondelle, J., Krijnen, S., and Van Santen, R. A., *J. Catal.* **171**, 77 (1997).
15. Yaluris, G., Rekoske, J. E., Aparicio, L. M., Madon, R. J., and Dumesic, J. A., *J. Catal.* **153**, 54 (1995).
16. Brouwer, D. M., and Oelderik, J. M., *Recl. Trav. Chim. Pays–Bas* **87**, 721 (1968).
17. Sherwood, P., De Vries, A. H., Collins, S. J., Greatbanks, S. P., Burton, N. A., Vincent, M. A., and Hillier, I. H., *Faraday Discuss.* **106**, 79 (1997).
18. Brändle, M., and Sauer, J., *J. Mol. Catal. A* **119**, 19 (1997).
19. De Vries, A. H., Sherwood, P., Collins, S. J., Rigby, A. M., Rigutto, M., and Kramer, G. J., *J. Phys. Chem. B* **103**, 6133 (1999).
20. De Gauw, F. J. M. M., Van Grondelle, J., and Van Santen, R. A., *J. Catal.*, in press.
21. Froment, G. F., and Bischoff, K. B., "Chemical Reactor Analysis and Design," p. 173. Wiley, New York, 1990.
22. Barrer, R. M., "Zeolites and Clay Minerals as Sorbents and Molecular Sieves." Academic Press, London, 1978.
23. Petersen, E. E., *in* "Catalyst Deactivation" (E. E. Petersen and A. T. Bell, Eds.), pp. 39–63. Dekker, New York, 1987.

24. Stull, D. R., Westrum, E. F., and Sinke, G. C., "The Chemical Thermodynamics of Organic Compounds." Robert E. Krieger Publishing Company, Malabar, 1987.
25. Eder, F., and Lercher, J. A., *J. Phys. Chem. B* **101**, 1273 (1997).
26. Eder, F., and Lercher, J. A., *J. Phys. Chem. B* **101**, 5415 (1997).
27. Haynes, H. W., Jr., and Sarma, P. N., *AIChE J.* **19**, 1043 (1973).
28. Van den Broek, A. C. M., Van Grondelle, J., and Van Santen, R. A., *J. Catal.* **167**, 417 (1997).
29. Kazansky, V. B., *Acc. Chem. Res.* **24**, 379 (1991).
30. Lercher, J. A., Gründling, Ch., and Eder-Mirth, G., *Catal. Today* **27**, 353 (1996).
31. Kondo, J. N., Liqun, S., Wakabayashi, F., and Domen, K., *Catal. Lett.* **47**, 129 (1997).
32. Juskelis, M. V., Slanga, J. P., Roberie, T. G., and Peters, A. W., *J. Catal.* **138**, 391 (1992).
33. Xu, L., Zhang, Z., and Sachtler, W. M. H., *J. Chem. Soc., Faraday Trans.* **88**, 2291 (1992).
34. Guillemot, D., Polisset-Thfoin, M., and Fraissard, J., *J. Phys. Chem. B* **101**, 8243 (1997).
35. Wang, H. T., Chen, Y. W., and Goodwin, J. G., Jr., *Zeolites* **4**, 56 (1984).
36. Blackmond, D. G., and Goodwin, J. G., Jr., *J. Chem. Soc., Chem. Comm.* **3**, 125 (1981).
37. Sachtler, W. M. H., and Stakheev, A. Yu., *Catal. Today* **12**, 283 (1992).
38. Sachtler, W. M. H., and Zhang, Z., *Adv. Catal.* **30**, 129 (1993).
39. Rödenbeck, Ch., Kärger, J., and Hahn, K., *J. Catal.* **176**, 513 (1998).
40. Denayer, J. F., Baron, G. V., Martens, J. A., and Jacobs, P. A., *J. Phys. Chem. B* **102**, 3077 (1998).
41. Eder, F., and Lercher, J. A., *Zeolites* **18**, 75 (1997).
42. Kazansky, V. B., Frash, M. V., and Van Santen, R. A., *Appl. Cat. A Gen.* **146**, 225 (1996).
43. Union Carbide Corporation, *Hydrocarbon Processing* **63**, 121 (1984).